107-116, North-Holland, New York.
Van Eldik, L. J., Grossman, A. R., Iverson, D. B., & Watterson, D. M. (1980) *Proc. Natl. Acad. Sci. U.S.A. 77*, 1912.
Van Heyningen, V., Craig, I., & Bodmer, W. (1973) *Nature (London) 242*, 509.
Walsh, K. A., Ericsson, L. H., & Titani, K. (1978) in *Versatility of Proteins* (Li, C. H., Ed.) pp 39-58, Academic Press, New York.
Walsh, K. A., Ericsson, L. H., Parmelee, D. C., & Titani, K. (1981) *Annu. Rev. Biochem. 50*, 261.
Waxdal, M. J., Konigsberg, W. H., Henley, W. L., & Edelman, G. M. (1968) *Biochemistry 7*, 1959.
Weitzman, P. D. J., & Danson, M. J. (1976) *Curr. Top. Cell. Regul. 10*, 161.
Wiegand, G., Kukla, D., Scholze, H., Jones, T. A., & Huber, R. (1979) *Eur. J. Biochem. 93*, 41.

Analysis of an Allosteric Binding Site: The Nucleoside Inhibitor Site of Phosphorylase *a*†

Stephen Sprang, Robert Fletterick,* Michael Stern, Daniel Yang,‡ Neil Madsen,§ and Julian Sturtevant‖

ABSTRACT: Glycogen phosphorylase is inhibited by a family of related compounds [purines, purine nucleosides, nucleotides, and certain heterocyclic compounds, e.g., flavin mononucleotide (FMN)] which bind to an allosteric site located at the surface of the enzyme 10 Å from the catalytic cleft at which glucose and glucose 1-phosphate are bound. The interaction of several such inhibitors, adenine, caffeine, adenosine, inosine, ATP, and FMN, with rabbit muscle phosphorylase *a* in the glucose-inhibited form has been examined by X-ray crystallographic (difference Fourier) analysis at 3.0- and 2.5-Å resolution. The dissociation constant (K_d) for all of these ligands was determined by kinetic analysis and, for FMN, by fluorometry. The $\Delta S°$ and ΔH for association of FMN to phosphorylase were derived from analysis of calorimetric data. We have synthesized the structural and thermodynamic data in order to arrive at a description of the energetics of the binding interaction and its specificity. The inhibitors associate with phosphorylase by forming an intercalative complex in which the heterocyclic ring system is stacked between the aromatic side chains of F285 and Y612. When they do so, the inhibitor stabilizes the same conformation of residues 282-286 which binds α-D-glucose, an inhibitor which demonstrates synergism with the purine ligands. No other significant hydrogen-bonded contacts are made with the enzyme, and any polar or charged groups of the ligand (ribose, ribose phosphate, or ribityl phosphate) are solvated at the protein surface. There does not appear to be a single particularly favored orientation of the heterocyclic ring dipole within its binding pocket nor is there a favored orientation for the polar moiety of the ligand at the surface of the enzyme. Association free energies range from 2.0 kcal (ATP) to 7.0 kcal (FMN), and the complete quenching of FMN fluorescence on binding suggests that the stacking interaction is quite strong. Calorimetric analysis of FMN binding reveals that both ΔH and $\Delta S°$ of association are significant. An unusual feature of the interaction is the strong temperature dependence of ΔC_p. Our analysis of the complex demonstrates that ΔG_d is not a simple function of the loss of accessible surface for protein and ligand upon binding. On the other hand, loss of accessible surface of the heterocyclic ring system alone correlates directly with ΔG_d. We conclude that the association energy derives solely from attractive dispersion forces in which both enthalpic and entropic contributions are significant. Accordingly, change in accessible surface on binding reflects both contributions to the free energy of binding.

Crystallographic analysis has revealed many examples of the intricate network of nonbonded interactions which characterize protein-ligand complexes. However, the balance of forces which confer stability or specificity to these interactions remains poorly understood. Such complexes have rather low free energies of association (3-10 kcal/mol) because they arise from the small differences among many individual entropic and enthalpic contributions of much greater magnitude. Structural analysis has allowed direct visualization of the role of electrostatics and complementarity. On the other hand, the static structure does not suggest the entropic contributions, viz., changes in translational and rotational degrees of freedom in protein, ligand, and solvent, that result from binding. Recent attempts have been made to evaluate entropic (hydrophobic) contributions from structural data by computing the solvent-accessible surface area (ΔA) lost by protein and ligand as a result of binding (Janin & Chothia, 1978). However, this prescription is based on thermodynamic analysis of phase equilibria in simple systems (Nozaki & Tanford, 1971) which bear little resemblance to the complex environment within a protein-ligand binding pocket (Hvidt, 1978). The real contributions of electrostatics or buried surface to stability can be more accurately evaluated if ΔH and ΔS can be directly determined for the systems of interest (Sturtevant, 1977). In this report, we discuss the results of a combined crystallographic and thermodynamic approach to describe the ener-

† From the Department of Biochemistry and Biophysics, School of Medicine, University of California, San Francisco, California 94143. *Received September 22, 1981; revised manuscript received January 14, 1982.* This work has been supported by grants from the Medical Research Council of Canada (to N.M.), the University of Alberta Computer Center, the National Institutes of Health (Grant AM 26081 to R.F. and Grant GM 04725 to J.S.), NIH Postdoctoral Traineeship (Grant AM 06293 to S.S.), the National Science Foundation (Grant PCM79-06000 to R.F.), and the Kroc Foundation.

‡ Present address: Department of Crystallography, University of Pittsburgh, Pittsburgh, PA.
§ Present address: Department of Biochemistry, University of Alberta, Edmonton, Alberta, Canada T6G 2H7.
‖ Present address: Department of Chemistry, Yale University, New Haven, CT 06510.

0006-2960/82/0421-2036$01.25/0 © 1982 American Chemical Society

Table 1: Data Collection Parameters for the Ligand Binding Studies

ligand	concn (mM)	no. of crystals	total reflections	unique reflections	resolution (Å)	R^a	lattice constants[b] (Å)	rms $\Delta F/F^c$ (%)
caffeine I	2.0	51	44 009	21 599	2.5	0.025	128.0, 116.4	14.0
caffeine II	2.0	18	20 215	12 171	2.5	0.027	128.3, 116.7	12.0
adenine	4.0	6	9 044	8 751	3.0	0.026	128.1, 116.5	4.8
adenosine	1.0	6	8 561	7 976	3.0	0.026	128.3, 116.5	3.9
ATP	20.0	14	16 398	12 615	2.5	0.022	128.2, 117.0	6.0
inosine	15.0	9	11 165	10 351	2.5	0.035	128.2, 116.4	5.0
FMN	0.5	15	16 809	11 571	2.5	0.049	128.2, 116.5	7.0

[a] A set of common scaling reflections is measured for each crystal (data set); the agreement among sets is given by the merging index: $R_{merge} = \Sigma_{hkl}\Sigma_I {I_{hkl}}^i - \bar{I}_{hkl}/(\bar{I}_{hkl})$ where ${I_{hkl}}^i$ are the scaled intensities for the ith crystal and $\bar{I}_{hkl}$ is the mean. [b] The parent crystals are of the space group $P4_32_12$ with lattice constants a, b = 128.3 Å and c = 116.5 Å. [c] The root mean square change is observed scattering amplitude with respect to parent crystals.

getics and structure of a relatively simple effector site in a very complex enzyme.

Glycogen phosphorylase from muscle is inhibited by an allosteric effector which binds at a locus 10 Å from the catalytic site (Kasvinsky et al., 1978a,b). An extraordinary range of compounds binds at this, the "nucleoside inhibitor" or "I", site, including a variety of purines, purine nucleosides, nucleotides, and certain dyes. The discovery of this effector site and the significance to the kinetics of phosphorylase catalysis and its role in glucose metabolism have been documented (Kasvinsky et al., 1978a,b; Sprang & Fletterick, 1979) and reviewed (Fletterick & Madsen, 1980). An important observation which emerged from these studies is the kinetic synergism between glucose and these inhibitors in promoting an inactive "T" conformation in phosphorylase. We have undertaken the structural analysis, by X-ray diffraction at moderate (2.5- or 3.0-Å) resolution, of several different crystalline complexes of phosphorylase *a* with inhibitor compounds [adenine, caffeine, adenosine, inosine, ATP, and flavin mononucleotide (FMN)]. This work has revealed a simple and elegant molecular mechanism for the observed glucose–purine synergism in addition to defining the nature of the binding interaction itself.

Muscle phosphorylase exhibits a remarkably relaxed specificity for ligands belonging to the group of I-site inhibitors. Dissociation constants for the compounds studied were measured kinetically and found to span a range of over 3 orders of magnitude. This relative lack of specificity suggests, and the structure itself demonstrates, that a single and nonrestrictive interaction is responsible for ligand stabilization. Because it has proven possible to accurately measure ΔH and $\Delta S°$ for the binding of one effector (FMN) by fluorescence titration and flow calorimetry, we are presented with the opportunity to evaluate a simple and structurally defined binding interaction in thermodynamic terms.

Glycogen phosphorylase *a* from rabbit muscle is inhibited in vitro by three different classes of physiological ligands. Fructose 1-phosphate or uridine diphosphate glucose acts at the active-site locus and competes with the substrates P_i or G-1-P by binding to an activated enzyme conformation (Fletterick & Madsen, 1980). Glucose also competes with these ligands, but by stabilizing the enzyme in an inactive conformation (Hers, 1976; Fletterick & Madsen, 1980). The third class of inhibitors is less well-defined. These are represented by purines (and certain analogues) which compete with G-1-P although binding at the nucleoside or inhibitor site (Kasvinsky et al., 1978a) 10 Å from the active-site locus. All evidence suggests that this site exists only in the inactive or glucose-inhibited conformation. Glucose and purines or analogues seem to stabilize the same conformation of the enzyme (Withers et al., 1979) and are synergistic (positive heterotropic) inhibitors (Kasvinsky et al., 1978a,b). The ligand specificity and physiological functions of this nucleoside site are not established.

In an attempt to define further the structure, specificity, and function of this inhibitor site, we present 2.5- and 3.0-Å resolution X-ray analysis of the binding of caffeine, adenine, adenosine, ATP, inosine, and FMN (riboflavin phosphate) to phosphorylase *a* crystals. Dissociation constants for these ligands are measured kinetically. The enthalpy and entropy of FMN binding are determined from fluorescence and flow calorimetry. The structural factors which may define the specificity of this binding site and the interactions of these ligands with the enzyme are described and analyzed.

Materials and Methods

Crystals of phosphorylase *a* (Fletterick et al., 1976) were generously supplied by S. Schekosky. The ligand and crystals were soaked for 12–24 h at the concentrations listed in Table I, at 22 °C. All chemicals were purchased from Sigma. The soaking solutions, buffered at pH 6.8, contained 10 mM magnesium acetate, 10 mM 2-[bis(2-hydroxyethyl)amino]-ethanesulfonic acid (Bes), 0.1 mM ethylenediaminetetraacetic acid (EDTA), 0.1 mM dithiothreitol (DTT), and 50 mM α-D-glucose.

The caffeine I difference electron density map was calculated for crystals soaked with 200 mM maltoheptaose in the same buffer as above. A second (caffeine II) difference electron density map was available from our heavy-atom work used in determining the 2.5-Å resolution structure as previously described (Sprang & Fletterick, 1979). (The role of caffeine in this experiment was to stabilize the crystals and minimize X-ray damage.)

The X-ray data were collected by using diffractometer methods as described before (Fletterick et al., 1976) with Syntex P21 and Nicolet P3F diffractometers. The results for the data processing and merging are given in Table I. The data measured for each case are the most intense 40–60% of the total observable reflections. The difference maps were calculated by using parent structure amplitudes for the enzyme with glucose bound. The phases we used were derived either from multiple isomorphous replacement (Sprang & Fletterick, 1979) or from the atomic model of the structure partially refined (crystallographic R = 0.30) with data extending to 2.1-Å resolution. The electron density maps were interpreted by using the (MMS-X) computer graphics system at the University of Alberta and the Evans & Sutherland E&S Picture System II at the University of California, San Francisco. Graphics and electron density fitting software used in this work was developed by the Computer Science Laboratory of the University of Washington (MMS-X) and by Oliver Jones at the University of California (PIG), San Francisco.

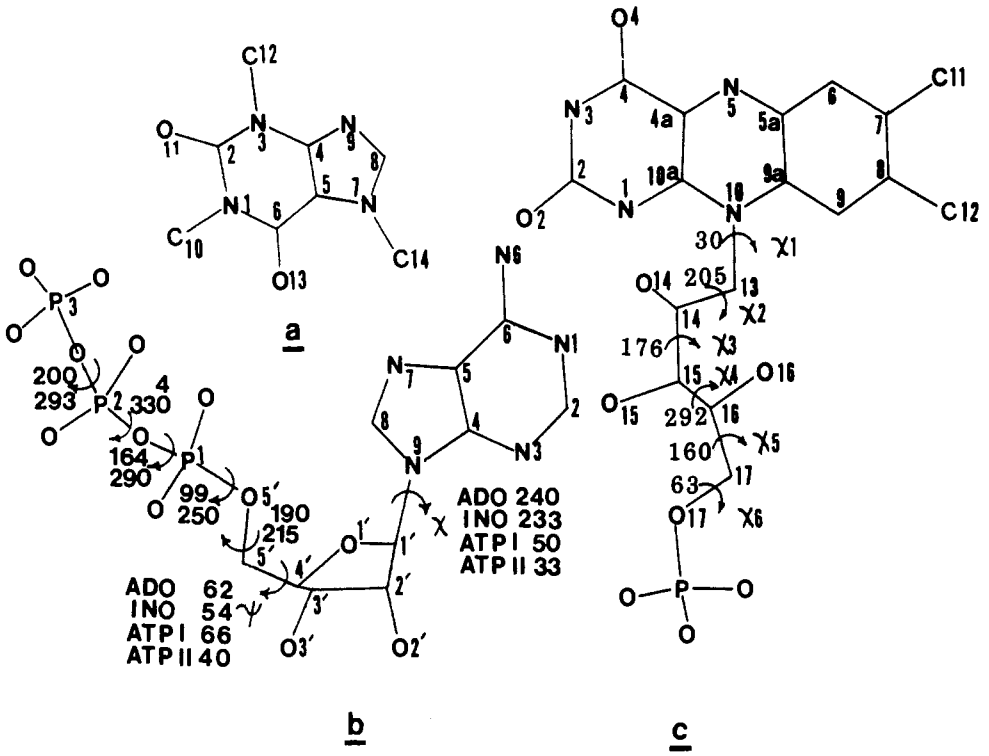

FIGURE 1: Atom numbering and conformational notation for the ligands. The numbering system for caffeine is given in (a), for adenine, adenosine, inosine, and ATP in (b), and for FMN in (c). Conformation angles determined from this study are listed beside a curved arrow about the bond of interest. Torsion angles are given with respect to intrachain atoms only. Note that χ [purine nucleosides (or nucleotides)] is defined with respect to the C8 and O1′ atoms, ψ with respect to C3′ and O5′, and χ_1 (FMN) with respect to CO9A and C13. The cis position is defined to be 0°. Conformation angles which are determined for more than one compound are listed beside the figure. ATP phosphodiester torsion angles are listed for both orientations I and II with those for I shown above those for II.

Molecular skeletal diagrams were prepared with the program CHEM by Andrew Dearing. Calculations of the solvent-accessible surface area as defined by Lee & Richards (1971) were carried out with a program written by T. J. Richmond. In computing the difference in solvent accessibility between bound and unbound ligand, we have assumed no conformation change in either ligand or protein. The solvent-accessible molecular surface is illustrated with the program MS designed and written by Connolly (1982).

Atomic coordinates for the ligands used to fit the difference electron density were taken from single-crystal X-ray diffraction studies: caffeine (Sutor, 1959), adenine and adenosine (Lai & March, 1972), inosine (Thewalt et al., 1970), ATP (Kennard et al., 1971), and FMN (Bear et al., 1973). Coordinates for the parent protein are from the latest partially refined set. The atom numbering systems used for the various ligands and the conformation angles determined from interpretation of the difference electron density maps are presented in Figure 1. The notations and conventions used for conformation angles of purine nucleosides and nucleotides are those of Pullman et al. (1973). The coordinates of the ligands with reference to the crystallographic unit cell are given in Table IV.

Kinetic Measurement of Dissociation Constants. Rabbit muscle phosphorylase *a* was prepared by the method of Krebs et al. (1964) as described previously (Kasvinsky et al., 1978a). Prior to use, the phosphorylase was dissolved and purified on a column of Sephadex G-25 (Kasvinsky & Madsen, 1976). Protein concentration of the purified enzyme was determined from absorbance measurements at 280 nm by using the absorbance index $E^{1\%}_{1cm}$ of 13.2 (Buc & Buc, 1968). Rabbit liver glycogen (type III), purchased from Sigma, was purified on a Dowex I-Cl column and assayed by the method of Dishe as described by Ashwell (1957).

Initial reaction rates were determined by the Fiske-Subbarow phosphate analysis in the direction of saccharide synthesis as described by Engers et al. (1970). Reaction mixtures were 0.5 mL and contained 2 mM sodium β-glycerophosphate (pH 6.8), 0.15 mM EDTA, 1 mM dithiothreitol, 28 mM glycol, 50 μg of serum albumin, and 2–4 μg of phosphorylase. Enzyme and glycogen were preincubated for 15 min at 30 °C before initiating the enzymatic reaction with glucose-1-P.

Fluorometric Titrations. The dissociation constant, K_d, of the phosphorylase–FMN complex was determined at 15–35 °C by fluorometric titration of the FMN by the enzyme. The fluorescence was exicted at 443 nm and observed at 538 nm, using a fluorometer based on a previously described stopped-flow apparatus (Sturtevant, 1964). The stopped-flow assembly was replaced by a 1 cm × 1 cm quartz cuvette mounted in a water-jacketed holder and equipped with an air-driven magnetic stirrer. Thermostating water was circulated through the jacket from a Lauda bath, and the temperature in the cuvette filled with water was checked by means of a calibrated AC2626 probe (Analog Devices, Norwood, MA). The titrations were run in buffer containing 10 mM sodium β-glycerophosphate, 1 mM EDTA, 1 mM dithiothreitol, and 50 mM α-D-glucose, pH 6.8.

For a typical titration, 10.0 mL of 10 μM FMN was placed in the cuvette, and 130 μM enzyme was added in amounts of 0.05–0.2 mL from a micrometer syringe. Fluorescence emission intensities were recorded on an arbitrary linear scale. About 15 readings were taken during each titration, and appropriate dilution corrections were applied. Care was taken to minimize the exposure of the solution to the exciting radiation.

Calorimetric Measurements. Enthalpies of binding FMN to phosphorylase were determined at 18, 25, and 35 °C in a flow calorimeter which has been previously described (Stur-

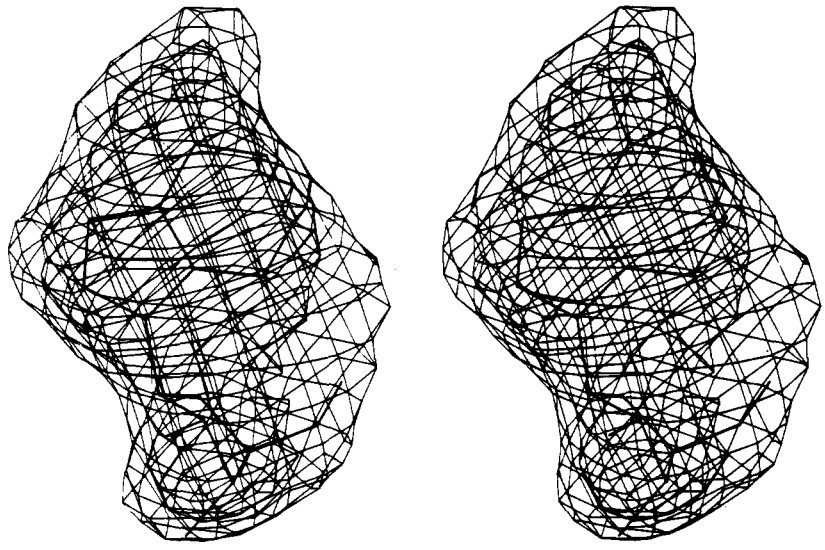

FIGURE 2: $F_{inosine} - F_{native}$ difference electron density calculated with diffraction data to 2.5-Å resolution. The cage contours are drawn at levels approximately 2 and 3 standard deviations above the mean map value. The model of inosine is shown superimposed on the density.

tevant & Lyons, 1969). Flow rates of 0.05–0.20 mL min^{-1} for each solution were employed, and flow times of 2 (for readings of total heat evolution) to 10 min for readings of the steady-state rate of heat evolution were employed. Enzyme concentrations of 100–150 μM and FMN concentrations of 50–1500 μM were used, in the same buffer as used in the fluorescence titrations, with omission of the dithiothreitol. Appropriate corrections were made for viscous heating and for enzyme and FMN dilutions.

Results

Crystallographic Structural Analysis. The difference electron maps for all ligands are generally of high quality; that obtained for inosine (Figure 2) is typical of the experiments.

Each of the ligands binds to the inhibitor site by forming an intercalative complex with a tyrosine and a phenylalanine, Y612 and F285. Inhibitors with purine moieties are bound such that the six-membered ring of the purine moiety lies directly between and approximately parallel to the ring planes of these two protein residues. This kind of protein–ligand interaction is not very common, but Rossmann et al. (1975) have reported that the adenine of NAD binds to glyceraldehyde-3-phosphate dehydrogenase in a stack composed of F34 and F99. The nature of the overlap for each ligand is illustrated in Figure 3a–g. The several ligands exhibit wide variation in the orientation of the base in the stacking plane. However, there is little variation in the interplanar ring separation or in the angle of tilt from the stacking plane. The mean separation between the six-membered ring center and the centers of the Y612 and F285 rings is 3.3 ± 0.2 and 4.0 ± 0.2 Å, respectively. The variation in the angle made by the purine ring with the Phe or Tyr rings is quite small, ca. 3°. The accuracy of these quantities is subject both to error in the model (about 0.3 Å in atomic position) and to changes in the parent structure induced by ligand binding.

With the exception of the stacking interaction, there is no common or analogous set of ligand–protein contacts which characterizes the inhibitors as a group in their interaction at the binding site. Ligands with ribose, ribose phosphate, or ribityl phosphate groups are bound with the polar or negatively charged moieties well solvated at the protein surface, although the orientation of the polar group is not the same for all ligands. In general, no hydrogen bonds are observed between the sugar or sugar phosphate groups and the protein.

The inhibitor binding site is located at the surface of the enzyme, less than 10 Å from and directly external to the active-site cavity where glucose is bound in the inactive conformation (Figure 4). There are six charged residues within 10 Å of the binding locus: D283, D287, E381, E571, D768, and R769. All but D283 are solvent accessible, and two (E381 and R769) form an ion pair. The aromatic residues involved in the stacking interaction, F285 and Y612, are themselves exposed at the surface of the protein. The ligand–protein complex effectively buries the internal, hydrophobic surface formed by the residues as illustrated in the molecular surface plot shown in Figure 5. Here, the molecular surfaces of ligand and protein have been calculated separately and then superimposed in the figure. The overlap of the surfaces demonstrates a contact between the ring planes of caffeine and Y612 less than the sum of the van der Waals radii of the involved atoms, and approximately 0.5 Å greater than the van der Waals sum for caffeine and F285. The binding site residues in the presence of three representative ligands, caffeine, inosine, and FMN, are depicted in Figure 6a–c. These residues lie at the entrance to the catalytic site tunnel (Figure 4).

Protein conformation changes due to binding inhibitor to either native or parent crystals are subtle and difficult to characterize at the resolution of the diffraction data used in this study. The position of Y612 determined from analysis of the parent structure would result in steric conflict and a slightly off-parallel stacking interaction with the base moiety of the ligand. We note that this residue as well as F285 is associated with weak difference electron density. However, the details of the structural changes by which the protein accommodates its ligand cannot be determined from these data. The most notable protein conformation change appears to be a retreat of H570 from the inhibitor locus toward the active-site cavity.

Caffeine. The caffeine I difference map was calculated with structure factor amplitudes from the dimethylmercuric acid derivative which contained caffeine as a stabilizing agent (Sprang & Fletterick, 1979). The caffeine II map was derived from crystals containing glucose, maltoheptaose, and caffeine. The two maps are quite similar, and both could be interpreted with the caffeine in either of two orientations related by a rotation of ca. 180° about the long axis of the purine ring. We have chosen that shown in Figure 3b because it places the oxygen substituents in higher electron density than the methyl groups. In this orientation, the C10 methyl substituent of caffeine, rather than an oxygen, is positioned over the Y612

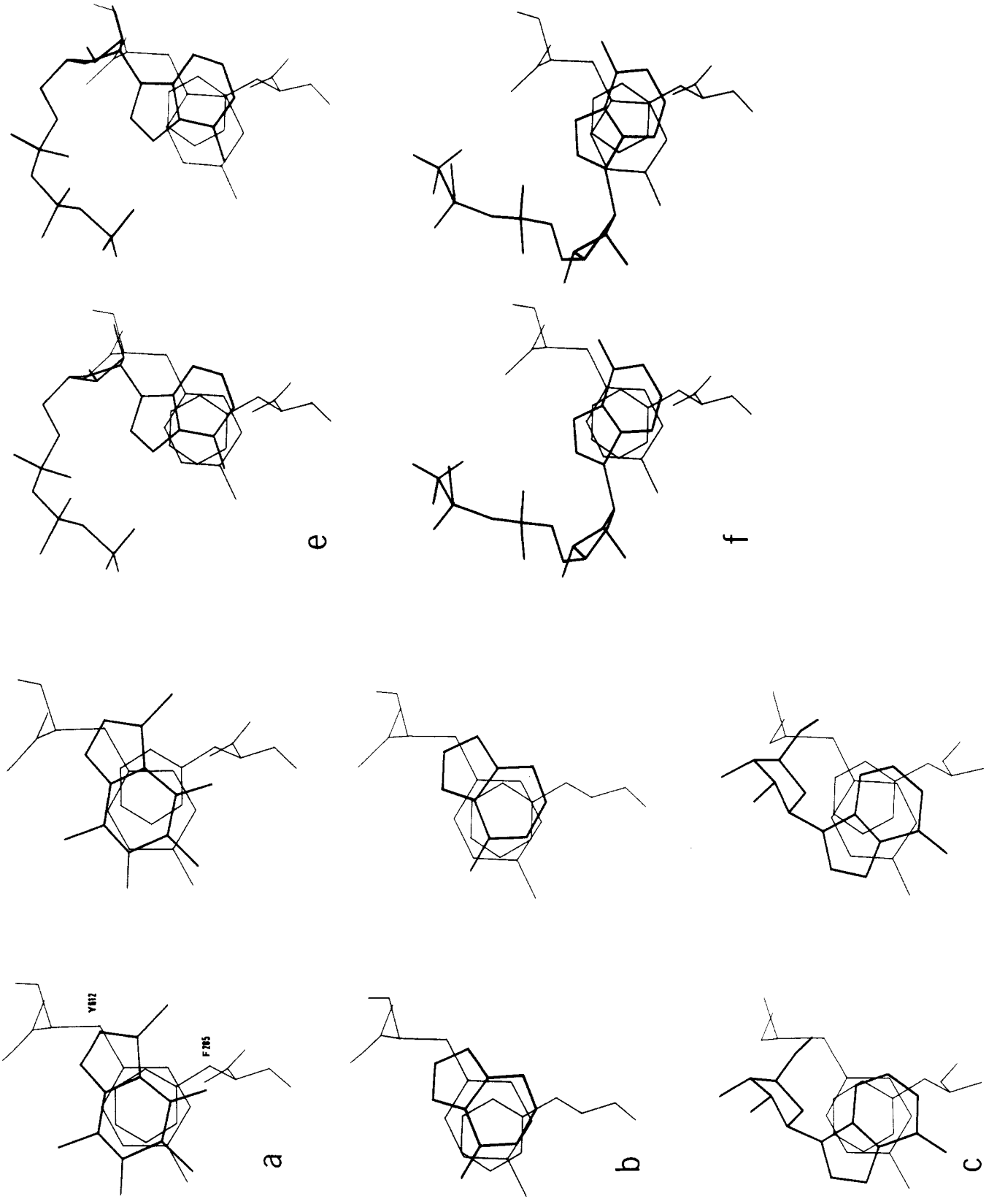
Y812
F785
a
b
c
e
f

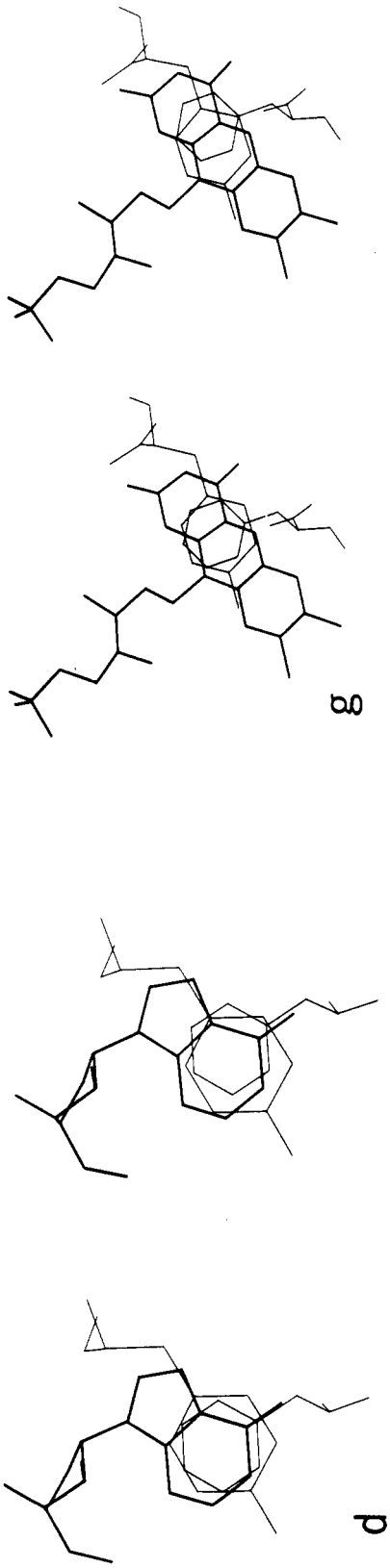

FIGURE 3: View of the stacking interaction involving inhibitor with F285 and Y612 taken approximately normal to the plane in which F285 and Y612 side chains are aligned. The drawing is rendered in perspective such that objects in the foreground appear relatively larger than background objects. (a) Adenine orientation I; (b) caffeine orientation I; (c) adenosine orientation I; (d) inosine; (e) ATP orientation I; (f) ATP orientation II; (g) FMN.

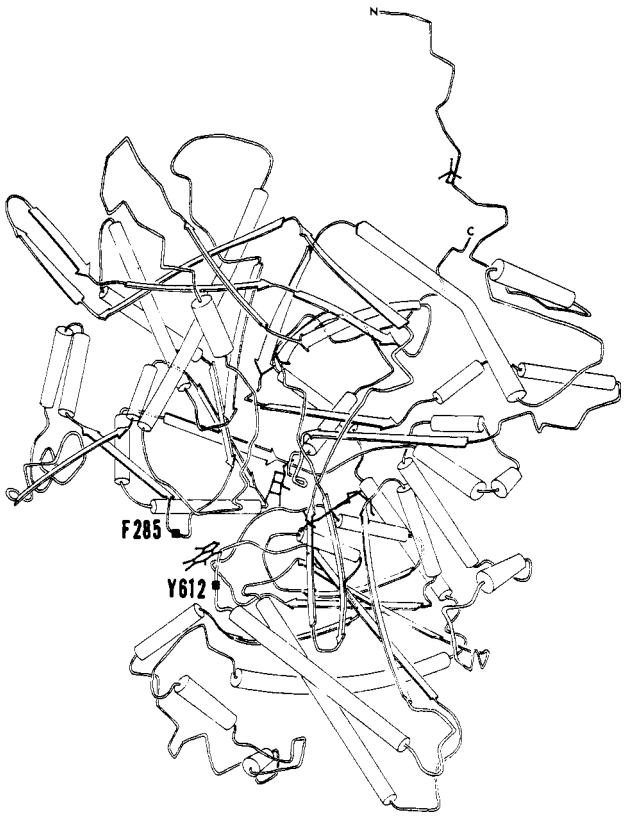

FIGURE 4: Schematic of the phosphorylase *a* monomer showing elements of secondary structure: helices as cylinders and β strands as arrows. Skeletal drawing of caffeine, glucose, and the covalently bound coenzyme pyridoxal phosphate are shown at the same scale. The approximate positions of the Cα atoms of the residues F285 and Y612 into which caffeine is intercalated are indicated with solid squares.

hydroxyl group. All atoms of the caffeine molecule but the O11 keto and C12 methyl substituents are solvent inaccessible. With the exception of the stacking residues, the closest caffeine–protein contacts are somewhat greater than the van der Waals distances.

Adenine. The adenine difference density can be interpreted with two ring orientations related by a 150° rotation about the major purine axis. The orientation (I) shown in Figure 3a offers only a marginally better fit to the data. Here, the C6–N6 bond makes a 90° angle with the tyrosine Cϵ–Oζ bond. Most of the atoms of the purine ring are buried in complex, although C2, N3, C8, and N9 are partially (ca. 10 Å^2/atom) solvent accessible. In the alternative orientation (II), the C6–N6/Cϵ–Oζ angle is about 45°, and the base is withdrawn more deeply into the binding pocket than in I. Only the N6 substituent is solvent accessible. In neither orientation are any contacts less than van der Waals distances made with the protein. It is possible that there the binding site can accommodate either adenine I or II, and the resulting density represents an average over the distribution.

Inosine. Inosine assumes a *syn*-glycosyl conformation with the ribose puckered in the C2′-endo range. The conformation about the C4′–C5′ bond is gauche, thereby allowing an intramolecular N3–O5′ hydrogen bond. The orientation of the base in the binding site (Figure 3d) is similar to that of the adenine orientation shown in Figure 3b and of caffeine (Figure 3a). The six-membered ring binds with the C6–O6 bond orientated 90° from the Cϵ–Oζ bond of Y612 and buried within the stack. None of the purine ring atoms are solvent accessible. In contrast, the ribose moiety is well solvated. We have compared the calculated solvent accessibility of the iso-

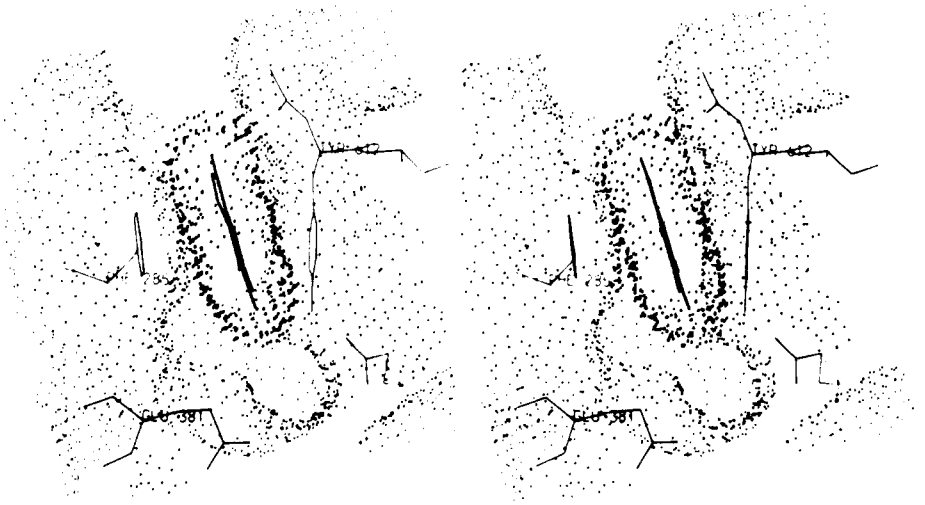

FIGURE 5: Space-filling diagram of the molecular surface of caffeine superimposed on that of the binding site residues (see text). The view is taken approximately along the line $x = y$ and perpendicular to the crystallographic c axis.

lated inosine molecule with inosine as bound at the inhibitor site (no change in inosine conformation is assumed) and find the difference in solvent-accessible surface area for the ribose to be 50 Å^2, or less than 6 Å^2 per ribose atom.

Adenosine. The difference electron density map for adenosine is of lower quality than that for the other ligands, particularly at the ribose moiety. The electron density suggests that adenosine may bind in either of two orientations related by a rotation about the long axis of the purine ring of ca. 180°. Consequently, there are two regions of electron density disposed at opposite ends of the purine density which correspond to alternative ribose positions. One of these, as shown in Figure 3c, is clearly stronger and represents the major adenosine orientation. The glycosyl conformation is unquestionably syn. The electron density could be reasonably well fit with the sugar in the C2′-endo conformation, as would be predicted by the results of extensive conformational analyses of purine nucleosides (Sundaralingam, 1975).

The orientation of the base (Figure 3c) is nearly perpendicular to that of the ligands discussed above. The major stacking overlap is centered predominantly over the six-membered ring with the C6–N6 bond orientated about 30° from the Y612 Cϵ–Oζ axis. All atoms of the purine but C8 are inaccessible to solvent.

The ribose moiety of adenosine is exposed at the surface of the binding site, but oriented toward the protein. The difference in accessible surface area of the ribose atoms between the free and bound adenosine is 130 Å^2, more than twice that obtained in the analogous calculation for inosine.

ATP. Like adenosine, ATP displays two alternative orientations in the binding site (Figure 3e,f), again related by a 180° rotation about the long axis of the purine ring. The boomerang-like electron density distribution is consistent with this interpretation. The electron densities for the two ribose moieties are not equally strong, suggesting that the two orientations are not equally populated (ATP I > ATP II). The triphosphate groups are poorly defined in the difference map because the phosphate positions for the two orientations overlap. Furthermore, the solvated triphosphate moieties appear to be conformationally disordered with respect to rotations about the β- and γ-phosphodiester linkages.

In both orientations, the ATP assumes an *anti*-glycosyl conformation and a C3′-*endo*-ribose pucker. The electron density at the ribose positions is not well-defined for all atoms of the sugar, but the equatorial O3′ atom is clearly evident for both orientations. The torsion angles about the C4′–C5′ and C5′–O5′ bonds are gauche–gauche and trans, respectively, in both orientations. These lie within preferred conformational ranges for 5′-nucleotides in the solid state (Sundaralingam, 1973) and in solution (Sarma, 1980). The alternative ATP orientations differ in conformation about the phosphodiester linkages, ATP I having a more extended triphosphate chain. The positions determined from the difference density map reflect only the most electron dense path; we assume that the strongest density is representative of the major conformer.

The orientation of ATP II in the binding site (Figure 3f) is similar to that of the major adenosine orientation (Figure 3c), although the base is buried more deeply in the binding pocket and tilted toward the enzyme. The C6–N6 bond is oriented along the Cϵ–Oζ bond of Y612, and the major stacking overlap is centered approximately over C6. The major, ATP I, orientation is unique among the other ligands studied here. Like ATP II, it is deeply withdrawn into the binding pocket such that the stacking overlap is centered on the C4–C5 bond. ATP in neither orientation makes extensive contact with the enzyme exclusive of the stacking interactions. The O2′ atom of ATP I is within 3.2 Å of Oϵ1 of E571 and the Y612 hydroxyl group. The ribose ring atom, O1′, of ATP I is less than 3.0 Å distant from the carbonyl oxygen of G611.

In both orientations, the adenine ring is completely inaccessible to solvent in the complex, though orientation I buries slightly more surface (ca. 20 Å^2) than II. The loss of accessible surface for the ribose triphosphate moiety is 100 (ATP I) or 130 Å^2 (ATP II). It is noteworthy that the orientation of minor occupancy is that resulting in the greater surface area lost for the base, and the lesser for the hydrophilic ribose triphosphate.

FMN. FMN exhibits the tightest binding to the phosphorylase inhibitor site (K_d = 2.5 μM) and the lowest inhibition constant (K_i = 5 μM) of the ligands we have studied. We have assumed a planar isoalloxazine ring (II) in our interpretation of the difference electron density. The dioxopyrimidine portion of the three rings lies in the strongest density, as do the ribityl atoms closest to the ring system. The density at the ribityl group diminishes as a function of the distance from the ring so that the phosphate at the terminus is very poorly defined. The phosphoribityl density is best interpreted with the carbon–carbon bonds alternating between trans (χ_2, χ_4, χ_6 = 180 ± 20°) and gauche (χ_3, χ_5 = 60 ± 20°) conformations. The ring–ribityl N–C bond (χ_1) exhibits a torsion angle of about 30°.

Within the binding pocket, the long axis of the isoalloxazine

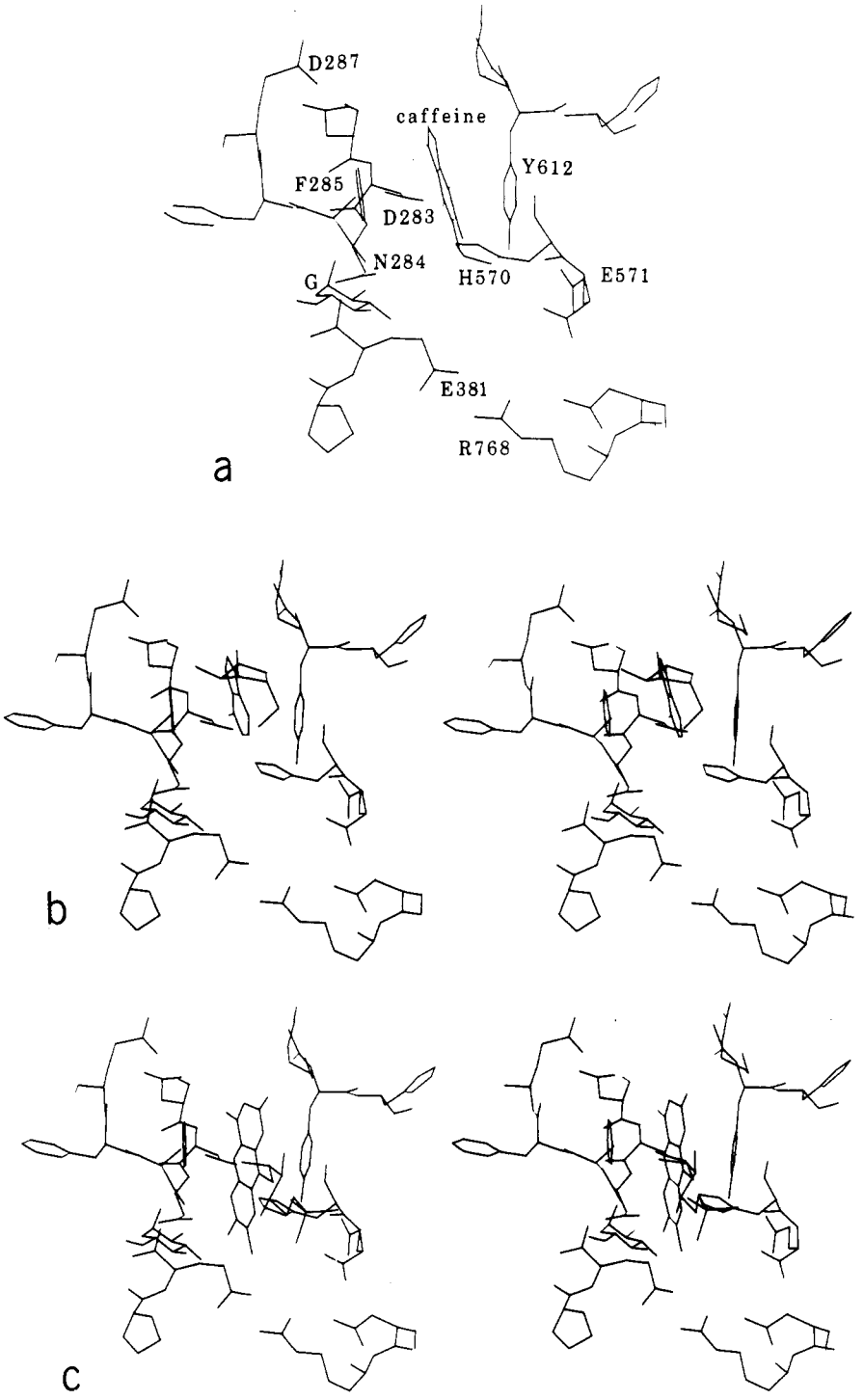

FIGURE 6: Modes of inhibitor binding in the presence of α-D-glucose, located within the catalytic site. Note the variation in the disposition of the polar moiety of the various ligands. The view is that shown in Figure 5: (a) caffeine orientation I, with the binding site residues numbered; (b) adenosine orientation I; (c) FMN.

is aligned with the axis defined by the Cδ1–Cε2 bond of F285, and so with the long axis of all of the purine ligands but adenosine and ATP. The stacking overlap extends predominantly over the central dioxypyrimidine ring of the isoalloxazine system such that the tyrosine Cε–Oζ bond projects over an area between the two nitrogen atoms of the central ring. The plane of the isoalloxazine ring is rotated by more than 20° (from the stacking plane defined approximately by the F285 and Y612 rings) with respect to the ring planes of the other purine derivatives. We infer that FMN causes a more significant perturbation of binding site residues than the other ligands.

None of the isoalloxazine ring atoms are accessible to solvent. We note that the methylated, hydrophobic end of the ring is associated with lower electron density than the remainder of the ring. It is possible there is some libration of the isoalloxazine system with the highest amplitude near the hydrophobic, methyl-substituted, end. The ribityl phosphate moiety appears to be almost completely solvated. The solvent accessibility difference between solvated and bound FMN, summed over the ribityl phosphate atoms, is less than 50 Å^2.

As with the majority of the ligands studied, FMN appears to make no productive contacts with the protein, exclusive of the stacking interaction. The closest of these, i.e., FMN C12–E381 Cγ (2.5 Å), FMN C6–H570 Cε1 (3.0 Å), and FMN O2–G611 O (2.6 Å), would be considered steric conflicts

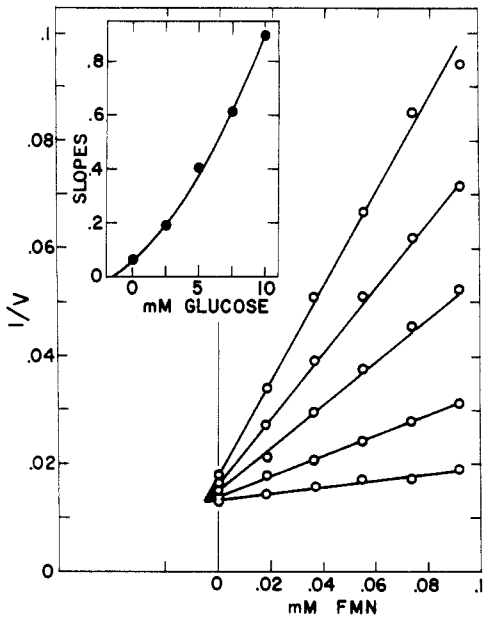

FIGURE 7: Dixon plot of reciprocal velocity (μmol min^{-1} mg^{-1}) vs. FMN concentrations at different glucose concentrations and 7.0 mM glucose-1-P. Glucose concentrations from lowest to highest sloped lines are 0, 2.5, 5.0, 7.5, and 10 mM. The intersection point is equivalent to an αK_i of 5 μM FMN. The replot of slopes vs. glucose concentration in the inset yields an αK_G of 1.3 mM glucose.

and would be alleviated by small conformation changes in the protein.

Determination of Dissociation Constants. As discussed in a previous paper (Kasvinsky et al., 1978b), glucose and compounds binding at the nucleoside inhibitor site affect phosphorylase *a* by a cooperative (synergistic) competitive inhibition in a nonexclusive manner. The nomenclature and treatment of data are according to Segel (1975) as applied before (Kasvinsky et al., 1978b): αK_G is the dissociation constant for glucose in the presence of saturating concentrations of the other inhibitor; αK_i is the dissociation constant for the inhibitor tested in the presence of saturating glucose, while α is the interaction constant between glucose and the other inhibitor.

A Dixon plot of reciprocal velocity vs. FMN concentration at increasing concentrations of glucose at fixed glucose-1-P (and saturating glycogen) concentration at 30 °C is presented in Figure 7. This plot demonstrates the nonexclusive interaction of the two ligands. An αK_i of 5 μM FMN may be calculated from the data while the αK_G is 1.3 mM but is less dependable due to the curvature of lines dependent on glucose concentration. A separate experiment in which both glucose and glucose-1-P concentrations are varied (data not shown) yielded a value for K_G of 3.5 mM from which an α of 0.43 may be calculated.

Experiments similar to that shown in Figure 7 were carried out with caffeine, inosine, adenine, and adenosine. The resultant values for αK_i and other constants are summarized in Table II. The αK_i for caffeine of 0.05 mM is similar to that of 0.06 mM obtained in the earlier experiments (Kasvinsky et al., 1978b). The K_d for ATP is difficult to measure kinetically so we estimate its value to be 10 ± 5 mM from occupancy analysis in difference maps at several concentrations.

Thermodynamic Analysis of FMN Binding. The thermodynamic parameters for the binding of FMN to phosphorylase *a* were evaluated from mutually consistent data obtained by fluorescence titrations and flow calorimetry. An equilibrium dissociation constant (K_d) was evaluated from each fluorescence titration on the assumption of equivalent and noninteracting binding sites with one site per 97 400 daltons. The fluorescence emission intensities observed after each addition of enzyme to FMN were fit with a least-squares analysis by using the initial intensity, the maximal fractional quenching (Q) of the fluorescence, and K_d as adjustable parameters. In 25 titrations, the mean value of the standard deviation of the observed intensities from the best curve was 8.5%. The mean value of Q was 0.941 ± 0.021 (standard deviation), with no detectable temperature dependence. It is unusual to observe such strong quenching, especially when the fluorescing material is being transferred from aqueous solution to a presumably nonpolar medium. The values obtained for K_d were used in a least-squares fit to the van't Hoff equation (Figure 8) including a temperature-independent value for ΔC_p, the heat capacity change in the binding reaction, and were found to fit the equation with a standard deviation of 15% in K_d. No improvement in the fit was obtained with ΔC_p taken as a linear function of the temperature. The value of K_d at 25 °C was 2.60 μM.

Table II: Kinetic Constants for the Interaction of Phosphorylase *a* with Various Ligands[a]

	adenine	adenosine	inosine	caffeine	FMN
αK_i	0.5	1.9	1.0	0.05	0.005
K_i	0.95	3.5	ND	0.1	0.01
calcd α	0.53	0.54		0.5	0.5
αK_g	1.2	1.5	1.5	0.9	1.3
K_g	ND	ND	3.5	ND	2.9
calcd α			0.43		0.45

[a] Dissociation constants at 30 °C are in mM; αK_i is the dissociation constant for the respective ligand with glucose-saturated enzyme, αK_G is the dissociation constant for glucose with enzyme saturated with the respective ligand, and α is the interaction constant between glucose and the respective ligand. ND, not determined.

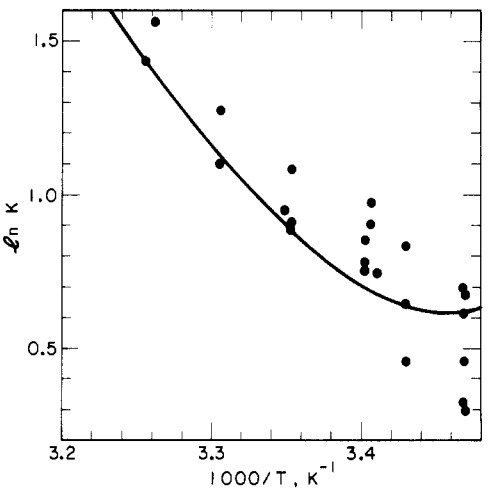

FIGURE 8: van't Hoff plot for the reversible association of FMN with phosphorylase *a*. The solid circles were determined from fluorescence titration. The solid line was determined by a least-squares fit of the calorimetric data to the van't Hoff equation with a temperature-dependent heat capacity term (eq 2). Seven enthalpy measurements were made at 18 °C, ten at 25 °C, and seven at 35 °C.

The calorimetric data gave clear indication of nonspecific binding of FMN to the enzyme, since the enthalpy of binding was found to increase with the total FMN concentration even at concentrations 2 orders of magnitude larger than the dissociation constant. It appears that this nonspecific binding makes no significant contribution to the fluorescence quenching. It was found, as illustrated in Figure 9, that the observed enthalpies, expressed as kilocalories per mole of

Table III: Thermodynamic Parameters for the Binding of FMN to Phosphorylase *a* in the Presence of 50 mM Glucose at pH 6.8

temp (°C)	K_d (μM)	$-\Delta G^\circ_u$[a] (kcal mol^{-1})	$-\Delta H$ (kcal mol^{-1})	$-\Delta S^\circ_u$[a] (cal K^{-1} mol^{-1})	$-\Delta C_p$ (cal K^{-1} mol^{-1})
15	1.88 ± 0.30	5.31 ± 0.70	−1.36 ± 0.70	−23 ± 2	1340 ± 100
20	1.98 ± 0.30	5.29 ± 0.09	4.56 ± 0.70	−2 ± 2	1030 ± 100
25	2.41 ± 0.36	5.24 ± 0.09	8.92 ± 0.70	12 ± 2	720 ± 100
30	3.22 ± 0.48	5.16 ± 0.09	11.7 ± 0.70	26 ± 2	400 ± 100
35	4.51 ± 0.68	5.05 ± 0.09	13.0 ± 0.70	26 ± 2	91 ± 100

[a] Unitary quantity (Gurney, 1953).

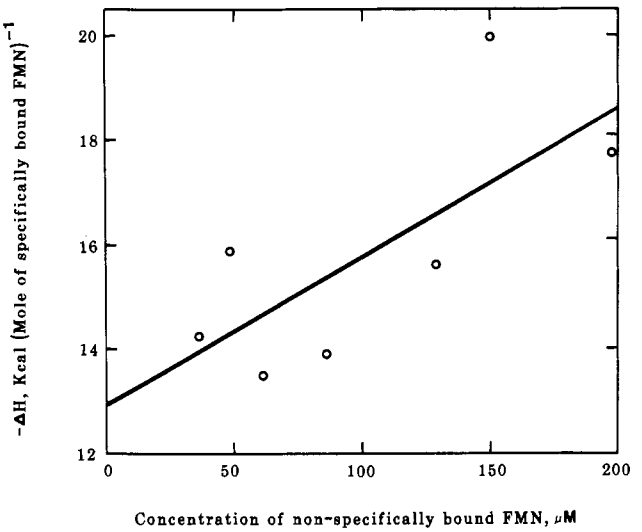

FIGURE 9: Enthalpies of binding of FMN to phosphorylase *a* in the presence of 50 mM glucose at pH 6.8, 35 °C. The fraction of the FMN present bound at the inhibitor site was calculated as outlined in the text. Concentrations after mixing in the calorimeter: enzyme, 84 μM; FMN, 110–280 μM.

specifically bound FMN, increased linearly with the concentration of *nonspecifically* bound FMN, the fluorometrically determined dissociation constants being used in the calculations. The intercept in a least-squares analysis at zero nonspecifically bound FMN is then the enthalpy of specific binding. The values obtained in this way were −2.37 ± 0.29, −8.92 ± 0.22, and −12.96 ± 0.60 kcal mol^{-1} at 18, 25, and 35 °C, respectively. The uncertainties given are standard errors. These values indicate an unusually strong dependence of ΔC_p on temperature, as expressed by

$$\Delta C_p = 2275 - 62.35t \text{ cal K}^{-1} \text{ mol}^{-1} \quad (1)$$

where t is the Celsius temperature. The average standard deviation calculated for the calorimetric data was ±0.9 kcal mol^{-1}, corresponding to ±0.07 mcal mL^{-1} of solution flowed through the calorimeter.

In general, calorimetry provides a better measure of enthalpy than do measurements of the temperature variation of equilibrium constants. Therefore, a consistent set of dissociation constants was obtained by using the integrated van't Hoff equation in the form appropriate for the case of ΔC_p varying linearly with temperature:

$$\ln K_d = \ln K_{298} - \frac{\Delta H_0}{R}\left(\frac{1}{T} - \frac{1}{298.15}\right) + \frac{A}{R}\ln\left(\frac{T}{298.15}\right) + \frac{B}{2R}(T - 298.15) \quad (2)$$

where ΔH_0 is formally the enthalpy change at 0 K, A and B are the constants in the equation $\Delta C_p = A + BT$, and T is the absolute temperature. The constants $\Delta H_0 = -2975$ kcal mol^{-1}, $A = 19\,305$ cal K^{-1} mol^{-1}, and $B = 62.35$ cal K^{-2} mol^{-1} were derived from the calorimetric data. A value of ln K_{298} was calculated from each titration value of ln K_d, a mean value for K_d at 25 °C of 2.41 ± 0.08 μM being obtained. This value is in fair agreement with the kinetically determined value given in Table II. The experimental values of K_d fit eq 2, with ln $K_{298} = 0.880$, with a standard deviation of 15%.

The thermodynamic quantities at 15–35 °C derived from the equilibrium constants calculated by means of eq 2 and the enthalpies listed above are given in Table III, with estimates of their uncertainties. The standard free energies and entropies are unitary quantities based on the unit mole fraction as the standard state for each species. In the calculation of these quantities, the usual approximation of setting standard enthalpies equal to observed enthalpies has been made.

Discussion

The results of this work bear on two fundamental and related problems: to account for the forces which stabilize specific protein–ligand (effector, substrate, or inhibitor) complexes and to determine the elements of the specificity. We cannot quantitatively attempt the first, because the initial and final structures of protein, ligand, solvent, and their complexes are not accurately known, nor can the changes in the dynamic range of structures in these components be described for the phosphorylase inhibitor site. The range of binding constants for the varied group of ligands is about 10^3, so the structural basis of specificity is likely to be subtle. Here, we attempt to synthesize the thermodynamic and structural results into a qualitative accounting of the energetics of binding.

Calorimetric investigation of the ΔH and ΔC_p of the inhibitor–phosphorylase interaction is hampered both by the low association constants for complex formation and by significant levels of nonspecific binding. These binding sites have not been observed crystallographically. FMN, due to its relatively high affinity for the inhibitor site, has proven to be the most tractable for calorimetry. Dissociation constants for the complex formed by the binding of FMN to the inhibitor site of phosphorylase, and the thermodynamic parameters for the formation of the complex, are given in Table III. As is to be expected in all cases where a large negative ΔC_p is observed, ΔH and $-T\Delta S^\circ$ are strongly temperature dependent in opposite directions while ΔG° is nearly constant, with the reaction changing from overall entropy drive at low temperature to overall enthalpy drive at higher temperature, undoubtedly with no change in the nature of the reaction. This sort of behavior is to be expected (Sturtevant, 1977) for processes which involve decreases in the exposure of hydrophobic groups to the aqueous solvent, increases in the exposure of charged groups to the solvent, or the change of easily excitable intramolecular degrees of freedom to higher frequency modes. In the present case, the first of these causes seems likely to be the most important. However, such considerations are complicated in this case by the fact that ΔC_p is itself a strong function of temperature, a complication which has seldom, if ever, arisen in previous studies.

The protein conformation changes which result from inhibitor binding to parent (glucose-bound) phosphorylase are

modest and predominantly local. NMR evidence suggests the structure of the enzyme is the same for caffeine bound as with glucose bound (Withers et al., 1979), and both visual and computational gradient analysis of the difference electron density suggests any structural changes on binding are very slight. This is in concert with the small differences we observe in structure amplitude on binding these ligands. (The exceptions are caffeine II and ATP where the enzyme is found to have other ligand binding sites filled.) While there is little conformational change apparent at 2.5-Å resolution, there are significant effects on the structure and dynamics of the molecule on binding ligands to one or both (glucose and nucleoside) sites, even in the crystals. Caffeine is known to block the accessibility of C142 to certain mercurials which attack this amino acid even in the presence of glucose (Sprang & Fletterick, 1979). This residue lies 30 Å from the glucose and purine binding sites. The most significant local structural change associated with binding is a shift of the H570 side chain toward the interior of the active-site pocket and closer to the D283 side chain. We may infer that the increase in the hydrophobicity of the H570 environment favors formation of an H570–D283 hydrogen bond or ion pair.

It is important that the inhibitors and glucose show synergistic inhibition of the enzyme (Kasvinsky et al., 1978b), or what is the same thing in this case, synergistic stabilization of the T conformation. It follows that the free energy of the T-state enzyme is lowered by the binding of inhibitor to the glucose–phosphorylase complex. The structural rationalization for this synergism is immediately evident upon examination of the parent–ligand complex (Figure 3a–c). Among the interactions made by glucose with the protein is a hydrogen bond between the glucose O2 and the N284 Nδ atoms (S. Sprang, S. B. Withers, R. J. Fletterick, and N. B. Madsen, unpublished experiments). The β turn formed by the sequence 282–286 also limits the accessibility of glucose to the solvent. The side chain of D283 occupies a "virtual" phosphate binding site and, by the negative electrostatic potential of the buried carboxyl group, prevents the binding of inorganic phosphate required for formation of an active, R, enzyme conformation. This sequence is conformationally mobile, and activators of the R state, like P_i, cause it to become disordered and, hence, dismantle the inhibitor site (Madsen et al., 1978). We explore this point elsewhere (S. B. Withers, N. B. Madsen, S. R. Sprang, and R. J. Fletterick, unpublished experiments). Caffeine stabilizes the T, glucose-bound conformation by anchoring the β-turn sequence to the protein surface and promoting the glucose–phosphorylase complex. We conclude that the inhibitor affects the phosphorylase structure not by changing the pattern of hydrogen bonds or ion pairs but by restricting or altering the conformational dynamics of the enzyme.

The conformation of the ligand itself may be important for inhibitors such as inosine, adenosine, ATP, and FMN which possess internal degrees of freedom which may be lost or restricted upon binding the enzyme. The effect may be more significant for the nucleosides and ATP for which rotation about the glycosyl or phosphodiester bonds may be hindered by binding. In purine nucleosides, the rotational barrier to the syn ↔ anti transition is low (Saran et al., 1973); the syn conformation, stabilized by the intramolecular hydrogen bond, is slightly favored (Sundaralingam, 1975). Thus, the conformation observed for inosine and adenosine in the binding pocket predominates in solution as well. At most, the enzyme may reduce somewhat the flexibility of the nucleoside and may account to a small degree for the higher K_d observed for these

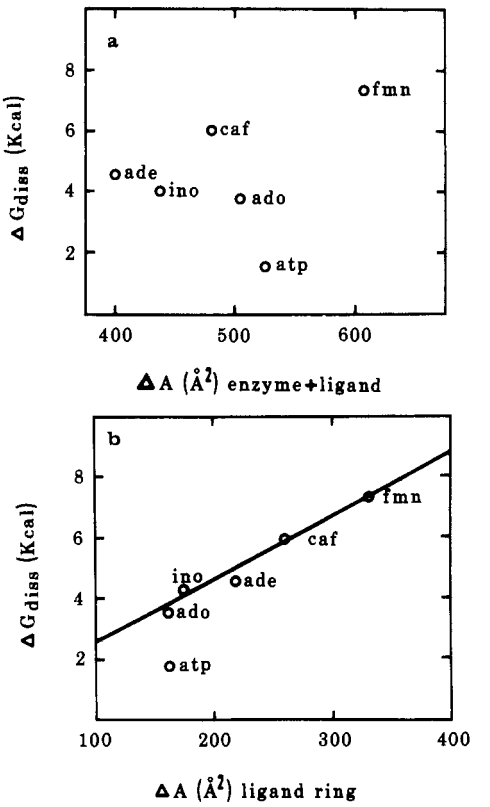

FIGURE 10: Plot of ΔG_d^{298} [calculated from αK_i given in Table III for caffeine (caf), adenine (ade), adenosine (ado), inosine (ino), ATP (atp), and FMN (fmn)] vs. the solvent-accessible surface area (Å^2) lost on complex formation for (a) both ligand and protein and (b) the base or conjugated ring system of the ligand only.

ligands. The anti conformation observed in both ATP orientations in the complex is known to be exclusively preferred by purine nucleotides in solution (Sarma, 1980) and in the solid state (Sundaralingam, 1975). Further, the C3′-*endo*-ribose pucker usually adopted by purine nucleotides in the "low" anti ($\chi < 50°$) conformation (Sundaralingam, 1975) obtains in the protein binding site as well. The enzyme does not perturb the ligand from its preferred equilibrium conformation. The effect of the enzyme upon the ribityl phosphate moiety of FMN is probably negligible because rotation about the ribityl bonds would not result in steric conflict with the enzyme.

Changes in solvent entropy have been explained (Kauzmann, 1959; Janin & Chothia, 1978) as liberation of ordered solvent from the hydrophobic surfaces of ligand and protein as a result of complex formation. It is important to note here that the hydrophobic effect, which describes the transfer of a hydrophobic group from water to an organic "solvent", is accompanied by a large negative change in heat capacity (Tanford, 1980). Consequently, both enthalpic and entropic effects are significant, but temperature dependent. The hydrophobic contribution is simply modeled by Janin & Chothia (1978), assuming no conformation change in ligand or protein upon binding, as the total difference in solvent-accessible surface area, ΔA (Å^2), as measured by the method of Lee & Richards (1971), between the complex and the isolated entities. We have computed this quantity for each ligand and graphed it against ΔG_d for that ligand (Figure 10a). A positive relationship might suggest that the hydrophobic effect, as modeled in this simple way, is important in stabilizing, and contributing specificity to, the complex. In fact, we observe such a correlation for adenine, caffeine, and FMN. However, the nucleosides and ATP are exceptions in that ΔG_d does not scale with the increased ΔA due to burial of the ribose or ribose

triphosphate atoms. We conclude that changes in total solvent accessibility cannot completely account for the relative free energies of binding in this system. Ross & Subramanian (1981) have discussed this point in detail.

Probably the most important source of binding energy is the ligand–protein interactions themselves. Here we refer to the enthalpic contributions arising predominantly from two sources: electrostatic (hydrogen bonding, charge pair) interactions and dispersion forces. The first of these does not appear to be important. Few of the ligands make hydrogen bonds with the protein, and there appears to be no advantage in binding energy (as expressed in the relative K_d's) for the ligands that do. All of the charged side chains within 10 Å of the purine binding site are relatively solvent accessible, and two (E381 and R769) are neutralized in a charge-pair interaction. Although the negatively charged groups lie more than 8 Å from the phosphate groups of ATP, they may account to some extent for the reduced affinity for nucleotides (Table II). However, we expect any charge effects to be small since negatively charged maleic acid ($K_d \simeq 200$ mM) and uric acid ($K_d \simeq 1$ mM) have been shown to bind to the inhibitor site (R. J. Fletterick and M. J. Stern, unpublished experiments). ATP also binds to an activator site and destabilizes the T conformation(s) of phosphorylase (see below). FMN binds with its terminal phosphate so well solvated that it may escape the effects of any local electrostatic field.

The forces operative in the interaction between the inhibitor and the protein residues F285 and Y612 are complex. The unusual and nearly complete quenching of FMN fluorescence on binding the nucleotide to phosphorylase suggests that the stacking interactions are very strong. It is not possible to make a thorough comparative study of the different complexes because the resolution of the X-ray data is limited and the conformation changes within the enzyme are not accurately characterized. We can suggest that the orientation of the conjugated ring within the stack and the extent of overlap contribute to the energetics and specificity of the interaction. The importance of these effects in the nucleic acid base interactions has been carefully investigated (Bloomfield et al., 1974). Among the phosphorylase inhibitors, there is a bimodal distribution in the angle made by the major axis of the ligand ring system with that of the Y612 phenol ring. It is likely the ring orientation is strongly influenced by other local interactions we have not characterized and by the steric restrictions imposed by the ribose or ribityl moieties. A straightforward measure of the extent of the stacking overlap is given simply by the loss of solvent-accessible surface area of the base atoms alone upon transferring the ligand from solvent to binding site. Given the flexibility of the ribose or ribityl moiety, it is also an estimate of the dynamic solvent accessibility change due to complex formation. We note that there is a significant variation in this quantity among the ligands and that it correlates strongly with the K_d of binding (Figure 10b). ATP is a notable exception to this correlation. Crystallographic analysis demonstrates that this compound binds at both the inhibitor site and the nucleotide activator site located near the subunit interface and causes a slight expansion of the unit cell along the c axis (Table I), typical of activators (Madsen et al., 1978). It is conceivable that ATP acts as a weak effector of the R state in solution and destabilizes the inhibitor site and raises the apparent K_d for binding at that locus.

We conclude that the major source of binding energy derives from the stacking interaction itself. The loss of solvent-accessible surface (ΔÅ^2) by the conjugated ring system alone is proportional to the free energy of binding and reflects both entropic and enthalpic components. The thermodynamic analysis of FMN binding demonstrates that both terms are significant. The broad specificity of this site in the muscle enzyme is explained by the predominance of a single and general source of stabilization, the attractive dispersion forces between the polarizable π systems of ligand and protein.

The physiological significance of relaxed inhibitor site specificity in the muscle enzyme is unclear. In contrast, phosphorylase from liver shows a more stringent selectivity for inhibitors (Kasvinsky et al., 1978b). It has been suggested (Kasvinsky et al., 1978a) that in vivo regulation of liver phosphorylase proceeds through a mechanism in which insulin promotes the release of a purine or purine nucleoside "second messenger" in response to changing glucose concentrations. Unlike the liver enzyme, muscle phosphorylase is probably not exposed to high or fluctuating levels of glucose under normal conditions (Kipnis et al., 1959) and may not be regulated by glucose–insulin synergism. The loss of specificity in muscle phosphorylase may reflect the absence of evolutionary pressure to maintain a selective inhibitor site.

Acknowledgments

We thank Ann Ma for excellent assistance in the calorimetric and fluorometric measurements and S. Shechosky for technical assistance in the performance of the kinetic analyses. We are grateful to Professor Peter Kollman for valuable discussions.

References

Ashwell, G. (1957) *Methods Enzymol. 3*, 73–105.
Bear, C. A., Waters, J. M., & Waters, T. M. (1973) *J. Chem. Soc., Perkin Trans. 2*, 1266–1271.
Bloomfield, V. A., Crothers, D. M., & Tinoco, I. (1974) *Physical Chemistry of Nucleic Acids*, p 22, Harper & Row, New York.
Buc, M. H., & Buc, H. (1968) in *Symposium on Regulation of Enzyme Activity and Allosteric Interactions*, p 109, Academic Press, New York.
Connolly, M. (1982) *QCPE* (in press).
Engers, H. D., Shechosky, S., & Madsen, N. B. (1970) *Can. J. Biochem. 48*, 746–754.
Fletterick, R. J., & Madsen, N. B. (1980) *Annu. Rev. Biochem. 49*, 31–61.
Fletterick, R. J., Sygusch, J., Murray, N., Madsen, N. B., & Johnson, L. N. (1976) *J. Mol. Biol. 103*, 1–13.
Gurney, R. W. (1953) in *Ionic Procession Solution*, McGraw-Hill, New York [reprinted by Dover Publications, New York (1962)].
Hers, H. G. (1976) *Annu. Rev. Biochem. 45*, 167–189.
Hvidt, A. (1978) *Biochim. Biophys. Acta 537*, 374–379.
Janin, J., & Chothia, C. (1978) *Biochemistry 17*, 2943–2948.
Kasvinsky, P. J., & Madsen, N. B. (1976) *J. Biol. Chem. 251*, 6852–6859.
Kasvinsky, P. J., Madsen, N. B., Sygusch, J., & Fletterick, R. J. (1978a) *J. Biol. Chem. 253*, 3343–3351.
Kasvinsky, P. J., Shechosky, S., & Fletterick, R. J. (1978b) *J. Biol. Chem. 253*, 9102–9106.
Kauzmann, W. (1959) *Adv. Protein Chem. 14*, 1–63.
Kennard, O., Isaacs, N. W., Motherwell, W. D. S., Coppola, J. C., Wampler, D. L., Larson, A. C., & Watson, D. B. (1971) *Proc. R. Soc. London, Ser. A 325*, 401–436.
Kipnis, D. M., Helmreich, E., & Coil, R. F. (1959) *J. Biol. Chem. 234*, 165–170.
Krebs, E. G., Love, D. S., Bratvold, G. E., Trayser, K. A., Meyer, W. L., & Fischer, E. H. (1964) *Biochemistry 3*, 1022–1033.

Lai, T. F., & Marsh, R. E. (1972) *Acta Crystallogr., Sect. B B28*, 1982–1989.
Lee, B., & Richards, F. M. (1971) *J. Mol. Biol. 55*, 379–400.
Madsen, N. B., Kasvinsky, P. J., & Fletterick, R. J. (1978) *J. Biol. Chem. 253*, 9097–9101.
Nozaki, Y., & Tanford, C. (1971) *J. Biol. Chem. 246*, 2211–2217.
Pullman, B., Saenger, W., Sasisekharan, V., Sundaralingam, M., & Wilson, H. R. (1973) *Jerusalem Symp. Quantum Chem. Biochem. 5*, 815–820.
Ross, P. D., & Subramanian, S. (1981) *Biochemistry 20*, 3096–3102.
Rossmann, M. G., Liljas, A., Branden, C. I., & Banaszak, L. J. (1975) *Enzymes, 3rd Ed. 2*, 61–102.
Saran, A., Perahia, D., & Pullamn, B. (1973) *Theor. Chim. Acta 30*, 31–44.
Sarma, R. H. (1980) in *Nucleic Acid Geometry and Dynamics* (Sarma, R. H., Ed.) p 145, Pergamon Press, Oxford.
Segel, I. H. (1975) *Enzyme Kinetics*, pp 481–492, Wiley-Interscience, New York.
Sprang, S., & Fletterick, R. J. (1979) *J. Mol. Biol. 131*, 523–551.
Sturtevant, J. (1964) in *Rapid Mixing and Sampling Techniques in Biochemistry*, pp 89–103, Academic Press, New York.
Sturtevant, J. M. (1977) *Proc. Natl. Acad. Sci. U.S.A. 74*, 2236–2240.
Sturtevant, J., & Lyons, M. (1969) *J. Chem. Thermodyn. 1*, 201–212.
Sundaralingam, M. (1973) *Jerusalem Symp. Quantum Chem. Biochem. 5*, 417–456.
Sundaralingam, M. (1975) *Ann. N.Y. Acad. Sci. 255*, 3–42.
Sutor, J. (1959) *Acta Crystallogr. 11*, 453.
Tanford, C. (1980) *The Hydrophobic Effect: Formation of Micelles and Biological Membranes*, 2nd ed., pp 18–21, Wiley, New York.
Thewalt, U., Bugg, C. E., & Marsh, R. E. (1970) *Acta Crystallogr., Sect. B B26*, 1089–1101.
Withers, S. G., Sykes, B. D., Madsen, N. B., & Kasvinsky, P. J. (1979) *Biochemistry 18*, 5342–5348.

Amino Acid Sequence of Chick Skin Collagen α1(I)-CB8 and the Complete Primary Structure of the Helical Portion of the Chick Skin Collagen α1(I) Chain†

John H. Highberger, Clare Corbett, S. N. Dixit, Wing Yu,‡ Jerome M. Seyer, Andrew H. Kang, and Jerome Gross*

ABSTRACT: The primary structure of chick skin collagen α1-CB8, the 279-residue CNBr peptide from the helical portion of the α1(I) chain, has been determined by automated amino acid sequence analysis of tryptic peptides of the maleylated and of the cyclohexanedione-treated material, of thermolytic peptides, and of a single 40-residue chymotryptic fragment. The sequence thus obtained showed 95% identity with that of the corresponding peptide from rat collagen. Completion of this work permits the assembly of the complete helical amino acid sequence of the chick skin α1(I) chain.

At the present time at least five genetically distinct types of collagen are recognized, although there are indications that additional forms may exist. Type I is by far the most common, making up the framework of most of the tissues of the animal body, but is especially characteristic of skin, tendon, and bone. The molecule consists of three α chains, each containing over 1000 amino acid residues in peptide linkage with no sequence repetition beyond 6 residues except for one short 9-residue stretch near each end (Hulmes et al., 1973). Two of these, the α1(I) chains, are identical, and one, the α2 chain, is different in amino acid sequence. The molecule is thus usually represented as $[\alpha 1(I)]_2\alpha 2$. Type II, or $[\alpha 1(II)]_3$, is the predominant protein of cartilage. Type III, $[\alpha 1(III)]_3$, occurs primarily in cardiovascular tissue, although it is also found in most loose connective tissues. The chain structure of type IV collagen found in basement membrane of several different tissues is still controversial, as is that of the so-called type V or A–B collagen.

Primary structural analyses of type I collagen available in the literature are still incomplete in that the published sequence of the complete α1(I) chain is a hybrid consisting of part rat and part calf skin (Hulmes et al., 1973; Bornstein & Traub, 1979). Portions of the sequence of skin collagen from human and guinea pig sources are also available (Fietzek et al., 1974; Clark & Bornstein, 1972). The amino acid sequence analysis of the α2 chain of calf skin is also complete, but as yet unpublished (P. P. Fietzek, personal communication). The complete amino acid sequence of calf skin type III (Fietzek et al., 1979; Dewes et al., 1979a,b; Bentz et al., 1979; Lang et al., 1979; Allmann et al., 1979) and human liver type III (Seyer & Kang, 1977, 1978, 1981; Seyer et al., 1980) has recently appeared in the literature, and a large portion of type II collagen is also published (Butler & Ponds, 1971; Butler et al., 1976, 1977).

With this publication of the cyanogen bromide peptide, α1-CB8, the amino acid sequence determination of the α1(I) chain of chick skin collagen, including the nonhelical amino-

† From the Developmental Biology Laboratory, Department of Medicine, Massachusetts General Hospital and Harvard Medical School, Boston, Massachusetts 02114 (J.H.H., C.C., W.Y., and J.G.), and the Veteran's Administration Medical Center and Departments of Biochemistry and Medicine, University of Tennessee Center for the Health Sciences, Memphis, Tennessee 38104 (S.N.D., J.M.S., and A.H.K.). *Received June 17, 1981; revised manuscript received November 24, 1981.* This is Publication No. 895 of the Robert W. Lovett Memorial Group for the Study of Diseases Causing Deformities. This work was supported by U.S. Public Health Service Grants AM 3564 and AM 16506 and Training Grant AM 07258 from the National Institutes of Health, The Janie Fund, The Gebbie Foundation, and the Medical Research Service of the Veterans Administration.

‡ Present address: Thermo Electron Corp., Woburn, MA.

0006-2960/82/0421-2048$01.25/0 © 1982 American Chemical Society